Proceedings of the Korean Nuclear Society Spring Meeting
Cheju, Korea, May 1996

Influences of Viscous Losses and End Effects on Liquid Metal Flow in Electromagnetic Pumps

Hee Reyoung Kim, Joon Ho Seo and Sang Hee Hong
Seoul National University

Suwon Cho
Kyonggi University

Ho Yun Nam and Man Cho
Korea Atomic Energy Research Institute

Abstract

Analyses of the viscous and end effects on electromagnetic (EM) pumps of annular linear induction type for the sodium coolant circulation in Liquid Metal Fast Breeder Reactors have been carried out based on the MHD laminar flow analysis and the electromagnetic field theory. A one-dimensional MHD analysis for the liquid metal flowing through an annular channel has been performed on the basis of a simplified model of equivalent current sheets instead of three-phase currents in the discrete primary windings. The calculations show that the developed pressure difference resulted from electromagnetic and viscous forces in the liquid metal is expressed in terms of the slip, and that the viscous loss effects are negligible compared with electromagnetic driving forces except in the low-slip region where the pumps operate with very high flow velocities comparable with the synchronous velocity of the electromagnetic fields, which is not applicable to the practical EM pumps. A two-dimensional electromagnetic field analysis based on an equivalent current sheet model has found the vector potentials in closed form by means of the Fourier transform method. The resultant magnetic fields and driving forces exerted on the liquid metal reveal that the end effects due to finiteness of the pump length are formidable. In addition, a two-dimensional numerical analysis for vector potentials has been performed by the SOR iterative method on a realistic EM pump model with discretely-distributed currents in the primary windings. The numerical computations for the distributions of magnetic fields and developed pressure differences along the pump axial length also show considerable end effects at both inlet and outlet ends, especially at high flow velocities. Calculations of each magnetic force contribution indicate that the end effects are originated from the magnetic force caused by the induced current ($\boldsymbol{u} \times \boldsymbol{B}$) generated by the liquid metal movement across the magnetic field rather than the one ($\boldsymbol{E}$) produced by externally applied magnetic fields by three-phase winding currents. It is concluded that since the influences of the end effects in addition to viscous losses are extensive particularly in high-velocity operations of the EM pumps, it is necessary to find ways to suppress them, such as proper selection of the pump parameters and compensation of the end effects.

I. Introduction

A great interest in the linear induction EM pumps has been given as an elemental device for circulating the sodium coolant in Liquid-Metal Fast Breeder Reactors. The EM pumps have the advantage over the mechanical pumps due to the fact that they have no rotating parts, which results in simplicity and convenience of maintenance and repair. The basic operational experiments on pilot linear induction EM pumps with various geometrical shapes have been carried out, and the practical applications have been made for the other areas of research like liquid metal chemistry. The linear induction EM pump gets the driving power from Lorentz's forces generated by the time-varying magnetic fields and the current induced in the electrically conductive liquid metal. Mathematical solutions for the driving forces are obtained by solving MHD equations of incompressible viscous flow coupled with Maxwell's equations under appropriate assumptions. It is found that the mechanical pressure gradients developed in the pump duct are given as a function of the slip including other pump variables. Since the pumping pressures are developed by Lorentz's forces experiencing viscous drag forces, viscous loss effects on the electromagnetically-developed liquid metal flow need to be

investigated. Generally, the Hartmann number given by the system scale length and magnetic field with viscosity and electrical conductivity is used as a measurement of viscous effect[1]. In the present work, direct comparison of $J \times B$ force with viscous force is carried out by analytical solutions obtained from related equations. The calculated results show, at the nominal conditions, that the pump performance can be analyzed by electromagnetic treatment due to negligible viscous effects. In addition to viscous loss effects, there are end effects at inlet and outlet of the EM pump due to finite pump length. It is known that braking forces by these end effects result in a reduction in the driving force of the EM pump. Solving Maxwell's equations analytically and numerically, radial(B_r) and axial (B_z) magnetic fields are found along the pump axial direction in the cases with and without end effects. respectively. Force density distributions obtained by calculations indicate that end effects are mainly due to the electromagnetic force caused by the induced current ($u \times B$) generated by the liquid metal movement across the magnetic field rather than the one (E) produced by externally applied magnetic fields by three-phase winding currents. In this paper, MHD flow and electromagnetic analyses on the annular linear induction EM pumps with flowrates of 40,000 ℓ/min and 60 ℓ/min are carried out by solving MHD and Maxwell's equations.

II. Analysis of Viscous Losses by MHD Laminar Flow Analysis

The driving power of the annular linear induction EM pump is generated from Lorentz's force given by products of magnetic field (B) and induced current (J) perpendicular to it. Electrically conductive liquid fluid also experiences viscous forces while being developed by Lorentz's force. Therefore, a real hydrodynamical pressure difference at both the ends of pump appears to be reduced by viscous forces. In this respect, an attempt has been made to obtain the expression for the pressure gradient mathematically by analyzing MHD equations coupled with Maxwell's field equation.

As shown in Fig.1, a typical annular linear induction EM pump has sloted external cores in which exciting coils are inserted to generate $J \times B$ force in the liquid metal flowing in the annular duct. But, to simplify the problem, the real pump core shape of is turned into a smooth core face replacing exciting coils by an equivalent current sheet to real coil arrangement[2] as depicted in Fig.2. A few more assumptions are introduced as follows.

1) The pump has an infinitely-long annular channel with an equivalent current sheet replaced by discrete primary windings slotted in the outer core.
2) All fields in the pump are axisymmetric ($\frac{\partial}{\partial \theta} = 0$) in view of cylindrical arrangement of the pump system.
3) The equivalent current sheet representing the three-phase currents(I) of continuous primary windings of N turns having pole pairs of p and pole pitch of τ is given by $J_a(r_2, z, t) = J_m e^{j(\omega t - kz)} \hat{\theta}$ where $J_m = 3\sqrt{2} k_w NI / p\tau$.
4) The sheet current produces traveling sinusoidal fields in the same form of J_a with angular frequency of ω and wave number of k for B, E and J.
5) Radial magnetic field (B_r) is uniform due to negligible skin effect in a narrow liquid metal gap[3].
6) The liquid metal flow is incompressible.

To analyze the system, first of all, MHD equations are needed for expressing conservations of fluid and momentum. The pressure gradient (∇P) arouses from the combined action of electromagnetic driving and hydrodynamic drag forces in the conducting fluid of density ρ, viscosity η, and fluid velocity u. Electromagnetic term by Lorentz's force is related with Maxwell's equations. Besides, induced current density (J) in the Lorentz's force is represented from Ohm's law given by electrical conductivity (σ) and fields ($E + u \times B$) induced both by traveling sinusoidal magnetic fields and conductive flow movement across them. Then governing equations are given as :

- MHD equations

$$\nabla \cdot u = 0$$

$$\rho\left\{ \frac{\partial \boldsymbol{u}}{\partial t} + (\boldsymbol{u}\cdot\nabla)\boldsymbol{u} \right\} = -\nabla P + \eta\nabla^2\boldsymbol{u} + \boldsymbol{J}\times\boldsymbol{B}$$

- Maxwell's equations

$$\nabla\times\boldsymbol{B} = \mu_o\boldsymbol{J} \qquad \nabla\times\boldsymbol{E} = -\frac{\partial \boldsymbol{B}}{\partial t}$$

$$\boldsymbol{B} = \nabla\times\boldsymbol{A} \qquad \boldsymbol{E} = -\frac{\partial \boldsymbol{A}}{\partial t}$$

$$\boldsymbol{J} = \sigma(\boldsymbol{E}+\boldsymbol{u}\times\boldsymbol{B})$$

In the MHD equations, we are interested in the time-averaged value of velocity. In practical sense, when velocity and flowrate are indicated, they generally mean the averaged values over time. Therefore, we will try to analyze the system in the time-averaged point of view. The time-averaged MHD equations are resulted in two reduced equations for flow velocity and magnetic field.

$$\frac{d^2\bar{u}}{d^2r} + \frac{1}{r}\frac{d\bar{u}}{dr} - a^2\bar{u} = \frac{1}{\eta}\frac{d\bar{P}}{dz} - a^2U_s$$

$$\frac{dB_z}{dr} = -\{\mu_o\sigma(-U_s+u)+j\}B_r$$

where

$$a^2 \equiv \frac{\sigma B_r^2}{2\eta} \quad , \quad U_s \equiv \frac{\omega}{k} \text{ (synchronous speed)}$$

B_r can be treated as a constant since radial magnetic field does rarely change at a narrow inter-core gap in induction machines having negligible skin effects. In general, magnetic core materials have very large permeabilities compared with those of liquid metals, and the differences of tangential magnetic fields between core($\boldsymbol{H}_1$) and liquid metal($\boldsymbol{H}_2$) regions are given by sheet current density($\boldsymbol{K}$) as

$$\boldsymbol{n}\times(\boldsymbol{H}_1-\boldsymbol{H}_2) = \boldsymbol{K}$$

Thus for the present pump model, we get

$$B_z(r_2) = \mu_o J_m \, , \quad B_z(r_1) = 0$$

Applying no-slip boundary conditions for velocity ($\bar{u}$) at the cylindrical walls(r_1, r_2), i.e., $\bar{u}(r_1) = \bar{u}(r_2) = 0$, we have solutions for the time-averaged velocity expressed in terms of the modified Bessel functions, I_o and K_o, of zeroth order as

$$\bar{u}(r) = \{AI_o(ar)+BK_o(ar)-1\}\left\{\frac{1}{a^2\eta}\frac{d\bar{P}}{dz} - U_s\right\}$$

where

$$A = \frac{K_o(aa)-K_o(ab)}{K_o(aa)I_o(ab)-K_o(ab)I_o(aa)}$$

$$B = \frac{I_o(ab)-I_o(aa)}{K_o(aa)I_o(ab)-K_o(ab)I_o(aa)}$$

If an average slip(s) over the channel gap is defined by

$$s \equiv \frac{1}{(r_2-r_1)}\int_{r_1}^{r_2}\left(1-\frac{\bar{u}}{U_s}\right)dr$$

The radial magnetic field(B_r) and axial pressure gradient ($\frac{d\bar{P}}{dz}$) are obtained as function of s together with other pump parameters.

$$B_r = \frac{\mu_o J_m}{(-\mu_o\sigma sU_s+jk)(r_2-r_a)}$$

$$\frac{dP}{dz} = \frac{1}{2}\sigma U_s B_r^2 \left\{ s + (1-s)\left[1 + \frac{1}{\frac{1}{r_2 - r_1}\int_{r_1}^{r_2} (AI_0(\alpha r) + BK_0(\alpha r) - 1) dr} \right] \right\}$$

The axial pressure gradient has been developed by two components, Lorentz's force and viscous term. The first term of right-hand side, $\frac{1}{2}\sigma U_s B_r^2 s$ is originated from the electromagnetic force density which is simply obtained by direct calculation of $\boldsymbol{J} \times \boldsymbol{B}$. The other terms of right-hand side correspond to viscous force density. To compare the viscous force density with electromagnetic force density, numerical values of pressure differences versus slip (or flowrate) are represented graphically in Fig.3 for a pump system with flowrate of 40,000 ℓ/min under a pressure difference of 15 atm. Fig.3 indicates that viscous force density is negligible compared with electromagnetic force density through all flowrate values except for near synchronous speed (s = 0). Practically induction pumps are not operated at near the synchronous speed with very low slip. Due to real hydraulic load like valve or piping system, such low slip value needs to be avoided so that the system can generate quite realistic developing force. Since EM pumps are generally operated at sufficiently high slip region to generate a considerable developing force overcoming heavy hydraulic pressure load (more than a few atms), the pump system analyses can be treated by electromagnetic analysis alone neglecting viscous effects. After all, it is thought that mechanical pressure gradient in the system can be replaced by electromagnetic force density ($\boldsymbol{J} \times \boldsymbol{B}$) alone.

III. Analyses of End Effects by Electromagnetic Theory

In the previous section, it is shown that EM pumps at nominal conditions can be analyzed by electromagnetic treatment. In this section, end effects caused by finite pump length are investigated from the results of calculated magnetic field and force density distributions. Applying linear induction motor theory with constant flow velocity, Maxwell's equations are to be solved analytically and numerically[4, 5].

III-1. Analytic Approach

To solve Maxwell's equations analytically, an equivalent current sheet model with a finite axial length as in the Fig.2 is used. Then, assumptions are the same in the MHD flow analyses of previous section except an infinite axial extension. Maxwell's equation represented by magnetic vector potential ($\boldsymbol{A}$) yields

$$\nabla^2 \boldsymbol{A} = \mu\sigma\left[\frac{\partial \boldsymbol{A}}{\partial t} - \boldsymbol{u} \times (\nabla \times \boldsymbol{A}) \right]$$

where

$$\boldsymbol{A} = A(r, z)e^{i\omega t}\,\hat{\theta} = R(r)\,Z(z)e^{i\omega t}\,\hat{\theta}$$

Taking the Fourier transforms with respect to z, we have

$$A(r, z) = \frac{1}{2\pi}\int_{-\infty}^{+\infty} \bar{A}(r, \zeta)e^{ikz} d\zeta$$

$$\bar{A}(r, \zeta) = R(r)\int_{-\infty}^{+\infty} Z(z)e^{-i\zeta z} dz$$

$$J(\zeta) = \int_0^L Je^{-ikz}e^{-i\zeta z} dz = \frac{iJ}{\zeta + k}\{e^{-i(\zeta+k)L} - 1\}$$

Then, a reduced field equation is resulted as

$$\frac{d^2R}{dr^2} + \frac{1}{r}\frac{dR}{dr} - \left(\frac{1}{r^2} + \alpha^2\right)R = 0$$

where

$$\alpha^2 = \zeta^2 + i\mu\sigma(u\zeta + \omega)$$

From the reduced equation, magnetic vector potential is obtained in terms of first (I_0, I_1) and second (K_0, K_1) kinds of modified Bessel functions of zeroth and first orders.

$$A(r,z)=\frac{i\mu J}{2\pi}\int_{-\infty}^{\infty}\frac{e^{-i(\zeta+k)L}-1}{\zeta+k}\frac{G(r,\zeta)}{aH(\zeta)}e^{ikz}d\zeta$$

where

$$G(r,\zeta) = K_0(ar_1)I_1(ar)+I_0(ar_1)K_1(ar)$$
$$H(\zeta) = K_0(ar_1)I_0(ar_2)-I_0(ar_1)K_0(ar_2)$$

Applying the residue theorem and the asymptotic expression of Bessel functions,

$$A(r,z) = \mu JA_{1,0}+\mu J\sum_{n=1}^{\infty}A_{1,n} \qquad (z<0)$$

$$A(r,z) = \mu J\frac{G(r,-k)}{a(-k)H(-k)}e^{-ikz}$$
$$+ \mu JA_{2,0}+\mu J\sum_{n=1}^{\infty}A_{2,n}^{-}+\mu J\sum_{n=1}^{\infty}A_{2,n}^{+} \qquad (0<z<L)$$

$$A(r,z) = \mu JA_{3,0}+\mu J\sum_{n=1}^{\infty}A_{3,n} \qquad (z>L)$$

where terms from residues at $\zeta_0^{\pm}$ are given by

$$A_{1,0} = \frac{\mu J}{r\ln(r_2/r_1)}\frac{e^{-i(k+\zeta_0^-)L}-1}{\zeta_0^-+k}\frac{e^{i\zeta_0^- z}}{\zeta_0^--\zeta_0^+}$$

$$A_{2,0} = \frac{\mu J}{r\ln(r_2/r_1)}\left[\frac{e^{-i(k+\zeta_0^-)L}}{\zeta_0^-+k}\frac{e^{i\zeta_0^- z}}{\zeta_0^--\zeta_0^+}+\frac{1}{\zeta_0^++k}\frac{e^{i\zeta_0^+ z}}{\zeta_0^+-\zeta_0^-}\right]$$

$$A_{3,0} = \frac{\mu J}{r\ln(r_2/r_1)}\frac{1-e^{-i(k+\zeta_0^-)L}}{\zeta_0^++k}\frac{e^{i\zeta_0^+ z}}{\zeta_0^+-\zeta_0^-}$$

and terms from residues at $\zeta_n^{\pm}$ ($n>0$) are obtained as

$$A_{1,n} = \frac{G(r,\zeta_n^-)}{a(\zeta_n^-)H'(\zeta_n^-)}\left[\frac{e^{-i(\zeta_n^-+k)L}-1}{\zeta_n^-+k}\right]e^{i\zeta_n^- z}$$

$$A_{2,n}^{-} = \frac{G(r,\zeta_n^-)}{a(\zeta_n^-)H'(\zeta_n^-)}\left[\frac{e^{-i(\zeta_n^-+k)L}}{\zeta_n^-+k}\right]e^{i\zeta_n^- z}$$

$$A_{2,n}^{+} = \frac{G(r,\zeta_n^+)}{a(\zeta_n^+)H'(\zeta_n^+)}\left[\frac{1}{\zeta_n^++k}\right]e^{i\zeta_n^+ z}$$

$$A_{3,n} = \frac{G(r,\zeta_n^+)}{a(\zeta_n^+)H'(\zeta_n^+)}\left[\frac{1-e^{-i(k+\zeta_n^+)L}}{\zeta_n^++k}\right]e^{i\zeta_n^+ z}$$

Using $I_0' = I_1$ and $K_0' = -K_1$,

$$H'(\zeta)=a'(\zeta)\{-r_1[K_1(ar_1)I_0(ar_2)+I_1(ar_1)K_0(ar_2)]$$
$$+r_2[K_0(ar_1)I_1(ar_2)+I_0(ar_1)K_1(ar_2)]\}$$

The vector potential $A(r, z)$ consists of three kinds of travelling waves along z characterized by three poles $-k$, ζ_0^-, and ζ_0^+. Noting that $k>0$, Re $|\zeta_0^+|<0$ and Im $|\zeta_0^+|>0$, and Re $|\zeta_0^-|>0$ and Im $|\zeta_0^-|<0$, $e^{i(\omega t-kz)}$ term represents a normal wave moving to +z , $e^{i(\omega t+\zeta_0^- z)}$ term is an

inlet-end-effect wave damping along $+z$ and $e^{i(\omega t+\xi_0 z)}$ term is an outlet-end-effect wave damping along $-z$, respectively. Taking curl of magnetic vector potential ($\boldsymbol{B} = \nabla \times \boldsymbol{A}$) yields radial and axial magnetic fields as shown in Figs.4 and 5. The magnetic fields are seen to be distorted at both ends of the pump due to end effects. The time-averaged driving force density is given by

$$\boldsymbol{F} = \overline{|\boldsymbol{J} \times \boldsymbol{B}|} = \frac{1}{2}[\sigma(-i\omega A + uB_r)B_r^*]$$

from which Fig.6 presents the calculated force density distributions in an EM pump of 60 ℓ/min. It appears in the figure that, at both entry and exit ends, the force densities are dropped rapidly in their values due to end effects. Especially, at the inlet region locally the force has opposite direction to the normal motion of liquid metal, and it is thought that such phenomena cause a reduction of a pump efficiency or thrust.

III-2. Numerical Approach

Fig.7 describes a numerical model for the realistic EM pump. In this model, three-phase currents flow in primary windings slotted in the outer core, and other assumptions are the same as in the previous analytic approach. A two-dimensional Maxwell equation for the vector potential is obtained as

$$\frac{\partial^2 A_\theta}{\partial r^2} + \frac{1}{r}\frac{\partial A_\theta}{\partial r} - \frac{A_\theta}{r^2} + \frac{\partial^2 A_\theta}{\partial z^2} = \mu\sigma\left(\frac{\partial A_\theta}{\partial t} + u\frac{\partial A_\theta}{\partial z}\right)$$

and it is solved by FDM with SOR iterative algorithm for an EM pump of 60 ℓ/min[6]. Fig.8 shows radial magnetic field distributions along the axial direction and Fig.9 shows pressure force distributions developed along the axial direction. In Fig.8, as expected, rippled sinusoidal traveling waves are shown reflecting real coil arrangements in core slots. In Fig.9, reversed end effect forces increase with increasing fluid velocity. Especially, in Fig.9(b), it is noted that the faster fluid velocity is, the larger pressure force is at all axial positions, especially at both ends, reversing forces due to induced fields by motion of liquid metal in the magnetic field. As a result, it is thought end effects are mainly due to induced force of $(\boldsymbol{u} \times \boldsymbol{B}) \times \boldsymbol{B}$ produced by liquid metal movement rather than that of $\boldsymbol{E} \times \boldsymbol{B}$ generated by external 3-phase windings.

IV. Conclusion

Calculated results of the MHD flow analysis shows that the viscous loss effects on producing pressure differences are negligible compared with electromagnetic driving forces except in the low slip region where the pumps operate with very high flow velocities comparable with the field synchronous speed. The closed-form solutions obtained from the Fourier transform method for the current sheet model reveal that the end effects due to finiteness of the pump length are formidable. The numerical computations performed by the SOR iterative method on a realistic EM pump model also show considerable end effects, especially at high flow velocities, which are originated from the magnetic force caused by $(\boldsymbol{u} \times \boldsymbol{B}) \times \boldsymbol{B}$ rather than $\boldsymbol{E} \times \boldsymbol{B}$. Since the influence of the end effects in addition to viscous losses are extensive particularly in high-velocity operations of the EM pumps, it is necessary to find ways to suppress them, such as proper selection of the pump parameters and compensation of the end effects.

References

[1] H. Branover, *Magnetohydrodynamic flow in ducts*, A John Wiley & Sons, New York, 1978.
[2] S. A. Nasar, *Linear motion electromagnetic systems*, A John Wiley & Sons, New York, 1985.
[3] Lawson. P. Harris, *Hydromagnetic channel flows*, A John Wiley & Sons, New York, 1960.
[4] S. A. Nasar, *Linear motion electric machines*, A John Wiley & Sons, New York, 1976.
[5] W. F. Ames, *Numerical methods for partial differential equations*, Academic New York, 1977.
[6] E. E. Kunhardt and P. F. Williams, "Direct solution of Poisson's equation in cylindrically symmetric geometry : A fast algorithm", J. of Comp. Phys., **57**, 403-414 (1985).

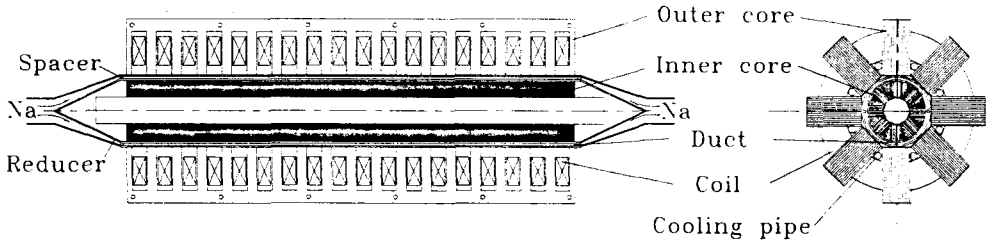

Fig. 1 Cross-sectional view of annular linear induction EM pump

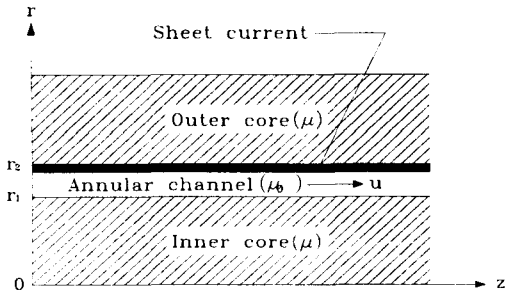

Fig. 2 Simplified laminar model with equivalent current sheet

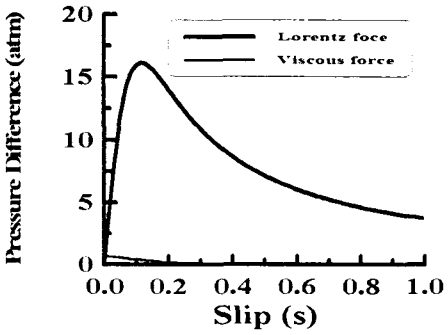

Fig. 3 Comparison of viscous force effects with Lorentz's ones on producing the pressure difference between the inlet and the outlet of a 40,000 l/min pump

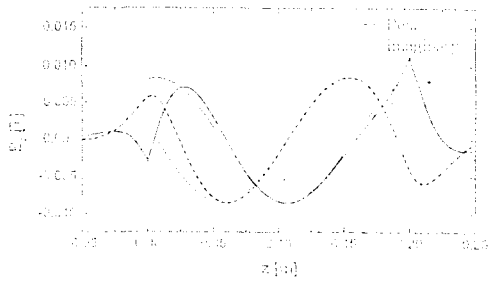

Fig. 4 Radial magnetic field distributions with (heavy curves) and without (light curves) end effects along pump axial direction

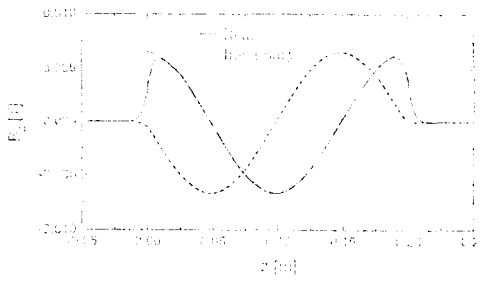

Fig. 5 Axial magnetic field distributions with (heavy curves) and without (light curves) end effects along pump axial direction

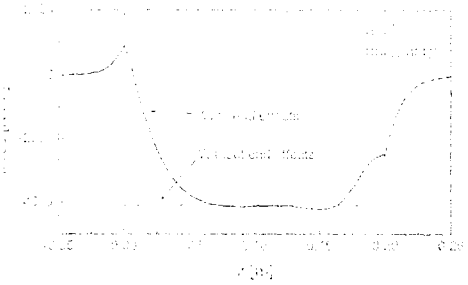

Fig. 6 Developing force distributions with (heavy curves) and without (light curves) end effects along pump axial direction

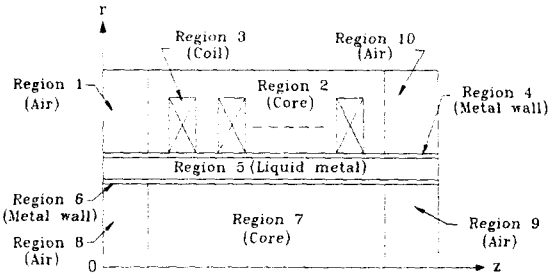

Fig. 7 Numerical model for realistic EM pump

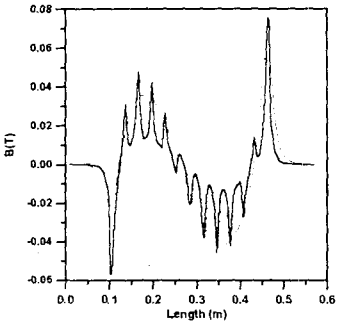

(a)

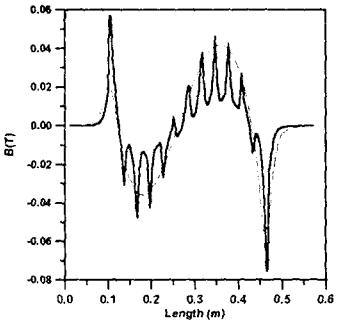

(b)

Fig. 8 Radial magnetic field distributions along pump axial direction computed numerically for a realistic discrete winding model (heavy curves) computed with those for an equivalent current sheet model (light curves) at (a) ωt = 0 ° and (b) ωt = 180 °

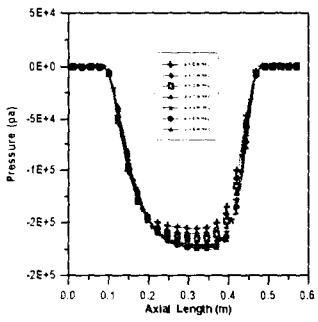

(a)

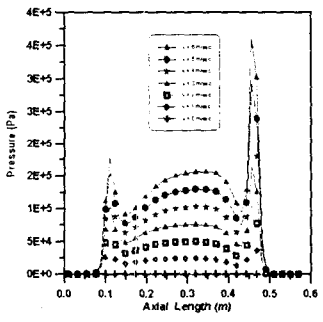

(b)

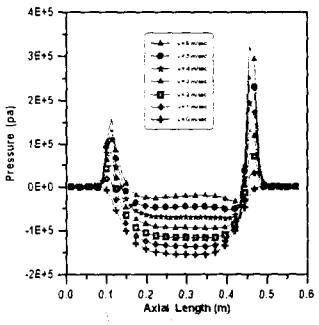

(c)

Fig. 9 Comparison of pressure distributions along the axial direction exerted by (a) $E \times B$, (b) $(u \times B) \times B$ and (c) total forces in the liquid metal of a 60 l/min pump operations with different flow velocities